ADVANCED ENERGY MATERIALS
www.advenergymat.de

All-Recyclable Triboelectric Nanogenerator for Sustainable Ocean Monitoring Systems

Junseong Ahn, Ji-Seok Kim, Yoonsang Jeong, Soonhyoung Hwang, Hyunjoon Yoo, Yongrok Jeong, Jimin Gu, Manmatha Mahato, Jiwoo Ko, Sohee Jeon, Ji-Hwan Ha, Hee-Seon Seo, Jungrak Choi, Mingu Kang, Chankyu Han, Yohan Cho, Chong Hyun Lee, Jun-Ho Jeong, Il-Kwon Oh,* and Inkyu Park**

The growing severity of environmental problems such as plastic waste and climate change has inspired active research into solutions based on recyclable and renewable energy devices. Triboelectric nanogenerators (TENGs) that convert wasted mechanical energy into electrical energy offer a solution that needs to be made recyclable to reduce or eliminate the generation of electronic waste (e-waste) on their disposal. In this study, an all-recyclable TENG (AR-TENG) based on a thermoplastic polymer with a nanohole pattern is developed; it delivers an excellent output power density of 1.547 W m^{-2} (peak output voltage = 360 V, current = 22 µA) and shows superior mechanochemical stability by maintaining its performance after immersion into seawater or 1 000 000 cyclic tests. The practical utility of this AR-TENG is demonstrated through its use to power a buoy-type ocean monitoring system and an intelligent life jacket, whereas recyclability is demonstrated by the re-fabrication of the AR-TENG; reusability in other devices is validated by the successful fabrication of a plasmonic color filter. This work paves the way for the efficient harvesting of renewable energy without the concomitant production of e-waste; therefore, it contributes to the mitigation of global environmental problems such as global warming and ozone depletion.

1. Introduction

Recent years have witnessed a revision in the international standards regulating greenhouse gas (e.g., carbon dioxide) emissions and an increased interest in the substitution of fossil fuels with renewable energy sources and the recycling of artificial materials.[1,2] Accordingly, many global companies have joined environmental campaigns such as Renewable Energy 100, and renewable energy harvesting devices and recyclable electronics have attracted considerable research attention.[3,4] Among such devices, triboelectric nanogenerators (TENGs) are of particular interest,[5] because they harvest renewable energy by converting wasted mechanical energy into electrical energy, and they are particularly efficient in harvesting the renewable energy of low-frequency mechanical motions such as that of water waves and human motion.[6] However, most existing TENG devices are neither recyclable nor eco-friendly, and thus, they present another mode of environmental pollution such as plastic and electronic wastes (e-wastes).[7]

Researchers have explored the use of recyclable materials in the manufacture of TENG components to address this e-waste problem. However, although such individual components can be reused, it is very difficult to recycle the integrated device itself because it is composed of several composite structures and it is difficult to be disassembled.[8–10] Further, methods to disassemble such composite structures require complicated steps which includes many environmental hazards.[11] to overcome this disassembling problem, researchers have recently developed soluble TENGs in which all (or some parts) of the device is completely water-soluble; however, this technology is limited by the fact that most electrode materials cannot be recycled because they are completely decomposed.[12,13] In addition, although the combination of water and water-soluble polymers is used for recycling because of its excellent eco-friendliness, the integration of water-soluble polymers in TENG makes it more vulnerable to humidity. Thus, it is difficult to use these devices in outdoor applications or water energy harvesting (e.g., ocean energy harvesting and rain energy harvesting), which is one of the most promising

J. Ahn, J.-S. Kim, H. Yoo, Y. Jeong, J. Gu, M. Mahato, J. Ko, J.-H. Ha, J. Choi, M. Kang, C. Han, I.-K. Oh, I. Park
Department of Mechanical Engineering
Korea Advanced Institute of Science and Technology (KAIST)
Daejeon 34141, Republic of Korea
E-mail: ikoh@kaist.ac.kr; inkyu@kaist.ac.kr

J. Ahn, S. Hwang, S. Jeon, J.-H. Ha, J.-H. Jeong
Department of Nano Manufacturing Technology
Korea Institute of Machinery and Materials (KIMM)
Daejeon 34103, Republic of Korea
E-mail: jhjeong@kimm.re.kr

Y. Jeong, C. H. Lee
Department of Ocean System Engineering
Jeju National University
Jeju 63243, Republic of Korea

H.-S. Seo, Y. Cho
Agency for Defense Development (ADD)
Changwon 51678, Republic of Korea

The ORCID identification number(s) for the author(s) of this article can be found under https://doi.org/10.1002/aenm.202201341.

DOI: 10.1002/aenm.202201341

applications of TENG.[14–17] The energy harvesting capacities of the currently developed recyclable TENGs are ≈10–100 times less than those of nonrecyclable TENGs because of the limitation of recyclable materials and structures.[18,19] Surface nanostructuring has been considered to increase the surface roughness and effective contact area;[20] however, poor long-term stability caused by damaged patterns from repeated shear and normal impacts hindered their practical applications to improve the performance of TENG. Developing both durable nanopatterns for high-performance TENGs and recyclable TENG devices for eco-friendliness remains as a challenging issue.

In addition, systems remotely operated in ocean environments should ideally contain self-powered sensor networks to avoid challenges associated with the periodic replacement of batteries and/or the direct measurements of ocean parameters by humans. Therefore, various buoy-type TENGs converting the motion of waves into electrical energy have been developed and used as power sources.[15,21–26] The development of mechanically and environmentally sustainable self-powered sensor networks for use in ocean environments relies on the availability of eco-friendly TENGs that have a long life span and can be stably operated for a long time.[27] However, this aspect has rarely been considered in recent studies. Conventional TENGs with micro- and nanostructured surfaces have excellent energy harvesting performance; however, they exhibit short life spans because of stress concentration-induced wear.[28,29] Further, most related studies are limited to electronics temporarily powered by a capacitor with a very fast discharge rate.[30,31] Therefore, the development of all-recyclable and disassembleable TENGs with high-performance power generation and mechanochemical stability remains challenging. In addition, the demonstration of ocean energy harvesting and monitoring systems is highly sought.

Herein, we developed an all-recyclable and mechanochemically robust TENG (AR-TENG) with a battery charging circuit and demonstrated its application to ocean energy harvesting and monitoring systems. The developed AR-TENG based on poly(methyl methacrylate) (PMMA) with a nanohole (NH) pattern and a Pd thin film relies on three strategies:

1) We selected PMMA and Pd as constituent materials to realize a mechanochemically stable yet recyclable TENG, while a NH pattern was selected as the structure of both contacting surfaces. The above materials are not easily oxidized or dissolved in aqueous solutions; however, they can be disassembled in acetone, which is one of the green solvents; therefore, TENG can be applied for water energy harvesting. The NH structure has a large moment of inertia against bending and a flat top surface that can uniformly distribute normal stress, and it is therefore mechanically stable with respect to the applied shear and normal stresses.
2) We used a simple bilayer structure, which allows the entire AR-TENG to be fabricated using only two materials (i.e., PMMA and Pd), to facilitate device disassembly. The abovementioned characteristics allowed the device to be easily disassembled and recycled by immersion into acetone.
3) We used Pd, which shows the best triboelectric properties in combination with PMMA among noble metals, as a counter electrode, and the surface nanopatterning of PMMA was conducted by nanoimprinting lithography (NIL) to improve the energy harvesting performance of the AR-TENG. The developed AR-TENG demonstrated superior energy harvesting performance, mechanochemical stability, and recyclability, which delivers an output power density of 1.547 W m^{-2} with a peak output voltage of 360 V and a current of 22 μA; it maintains high performance after immersion into seawater, 1 000 000 cyclic tests, or re-fabrication from recycled PMMA and Pd. **Figure 1**a shows the overall fabrication, recycling, and application processes. The broad applicability and recyclability of the fabricated AR-TENG were demonstrated through its disassembly and fabrication of a plasmonic color filter (PCF) using recycled raw materials. In addition, we developed an energy harvesting system with a battery charging circuit that can use the AR-TENG to charge a commercial Li-ion battery installed to drive electronics. We integrated this energy harvesting system into i) a wireless buoy-type sustainable ocean monitoring system equipped with pH, salinity, temperature, and oil leakage sensors and ii) an intelligent life jacket that could activate a global positioning system (GPS) sensor to send a position information signal in an emergency for demonstrating the practical applicability of this energy harvesting system. The ocean monitoring system based on our AR-TENG can be operated for a long time because of its battery charging systems with a low discharge rate and high mechanochemical stability. To the best of our knowledge, this is not only the first development of the green AR-TENG with the NH pattern that has high mechanical stability, but also the first demonstration of the integrated system of the ocean energy harvesting, battery charging, and ocean monitoring systems.

2. Results and Discussion

2.1. AR-TENG Fabrication

Unlike thermosets, thermoplastic polymers are easily recyclable because their chains do not degrade upon melting, i.e., the interactions between the chains of thermoplastic polymers are weaker than the chemical bonds between their monomer units. This property is beneficial for structuring and design, which allows for excellent formability at temperatures above the glass transition temperature (T_g).[32] Noble metals have outstanding chemical stability even at high temperatures and can therefore be easily extracted from integrated devices and reused. Herein, we exploited these material characteristics to fabricate the AR-TENG that utilizes a thermoplastic polymer (PMMA) as a substrate or a dielectric insulator and a noble metal (Pd) as an electrode or functional material. The PMMA was selected because of its formability, chemical resistance, weather resistance, UV resistance, abrasion resistance, high track and arc resistance, mechanical strength, and low cost, whereas Pd was selected because of its chemical stability and maximized triboelectric effect in combination with PMMA (Figure S1, Supporting Information). Two functional films, each comprising PMMA or Pd, were fabricated by UV-NIL, thermal NIL, and e-beam evaporation; a simple bilayer structure was selected to facilitate disassembly during recycling. The two bilayer films were used to construct the dielectric and conductor parts of the AR-TENG.

Figure 1b illustrates the fabrication process of functional films in more detail. We processed the PMMA film using a previously developed thermal NIL technique to enhance the performance of the AR-TENG[32] because TENG nanopatterning enhances the triboelectric performance by significantly increasing effective contact area and surface roughness.[33–35] Initially, a Si master mold was prepared (Figure 1b-i), and then, a nanopatterned polyurethane acrylate (PUA) mold was prepared by UV-NIL (Figure 1b-ii) and used to emboss two PMMA films by thermal NIL (Figure 1b-iii). In this process, PMMA becomes rubbery and therefore easily deforms under pressure at temperatures above T_g. For further details regarding the fabrication process, readers are referred to our previous research[32] and the experimental section. Subsequently, an e-beam evaporator was used to deposit a Pd thin film with a thickness of 50 nm on the back of one PMMA film (flat part) and the front of the other PMMA film (patterned part) as the electrodes of the dielectric and conductor parts of the AR-TENG, respectively (Figure 1b-iv). Figure 1c shows photographs of the dielectric and conductor parts of the AR-TENG, whereas Figure 1d and Figure S2 (Supporting Information) show the top- and side-view scanning electron microscopy (SEM) images of the conductor part of the AR-TENG. The PMMA is patterned by thermal NIL process and Pd with the thickness of 50 nm is deposited on both the top surface of the trench and the pillar of the nanopattern. In addition, the superior uniformity of the fabricated nanopatterned PMMA is described in Figure S3 (Supporting Information).

2.2. Structural Design and Characterization of the AR-TENG

Figure 2a shows a schematic of the AR-TENG, with its working mechanism and the related experimental setup presented in Figures S4 and S5 (Supporting Information). Figure S4a,b (Supporting Information) presents a schematic in the cross-sectional view and working principle of the AR-TENG, respectively, and Figure S4c (Supporting Information) provides electrostatic simulation that shows the working principle of the AR-TENG. The surface nanopatterning of PMMA by thermal NIL was used to enhance the triboelectric performance, and the effects of nanopatterning on each side of the AR-TENG were investigated in detail. The peak output voltage and current of the AR-TENG with a NH pattern on only one side were 1.4–1.8 and 4.2–4.6 times higher than those of the flat-surface AR-TENG, respectively. Further, the peak output voltage and current of the AR-TENG with an NH pattern on both sides were 2.05–2.6 and 1.8–2.0 times higher than those of the AR-TENG with an NH pattern on only one side, respectively (Figure 2b,c). The nanopattern type was optimized to achieve maximal triboelectric

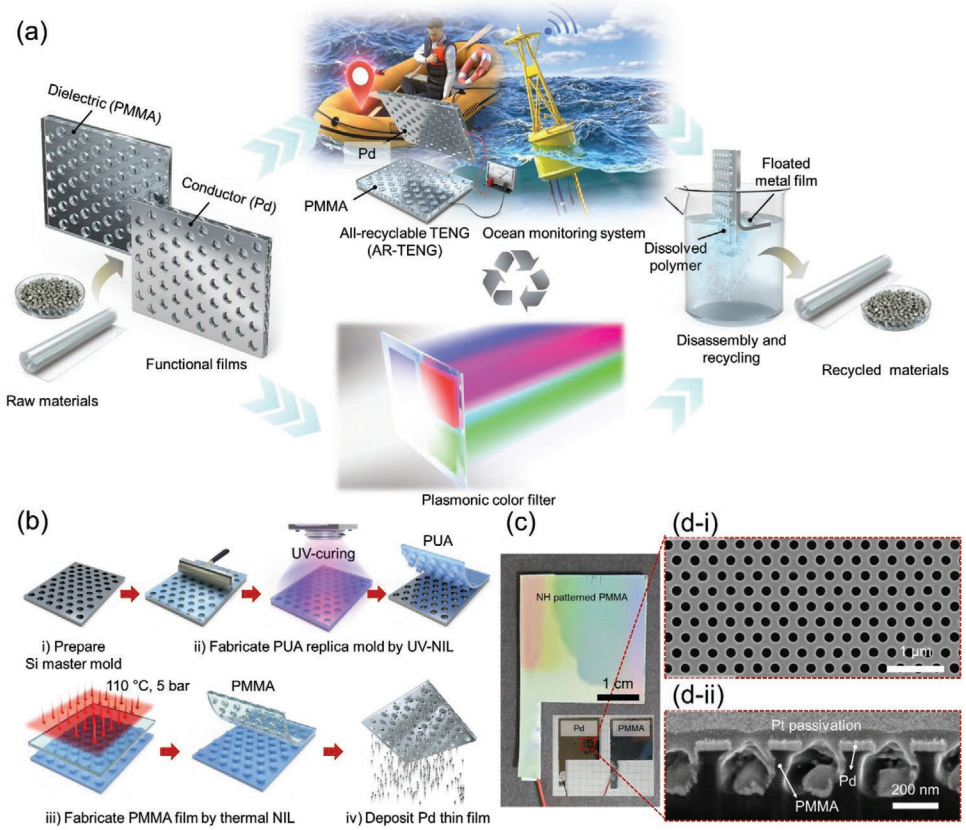

Figure 1. Schematic of a) AR-TENG recycling process and b) functional film fabrication by UV- and thermal NIL. c) Photographic images of fabricated AR-TENG, with the inset showing its dielectric (PMMA) and conductor (Pd) parts. The iridescent color different from the color of the surface material (PMMA) verifies the formation of periodic nanostructures on the surface. d-i) Top- and d-ii) side-view SEM images of the conductor part of AR-TENG. For the acquisition of the side-view image, the sample was sliced using a focused ion beam.

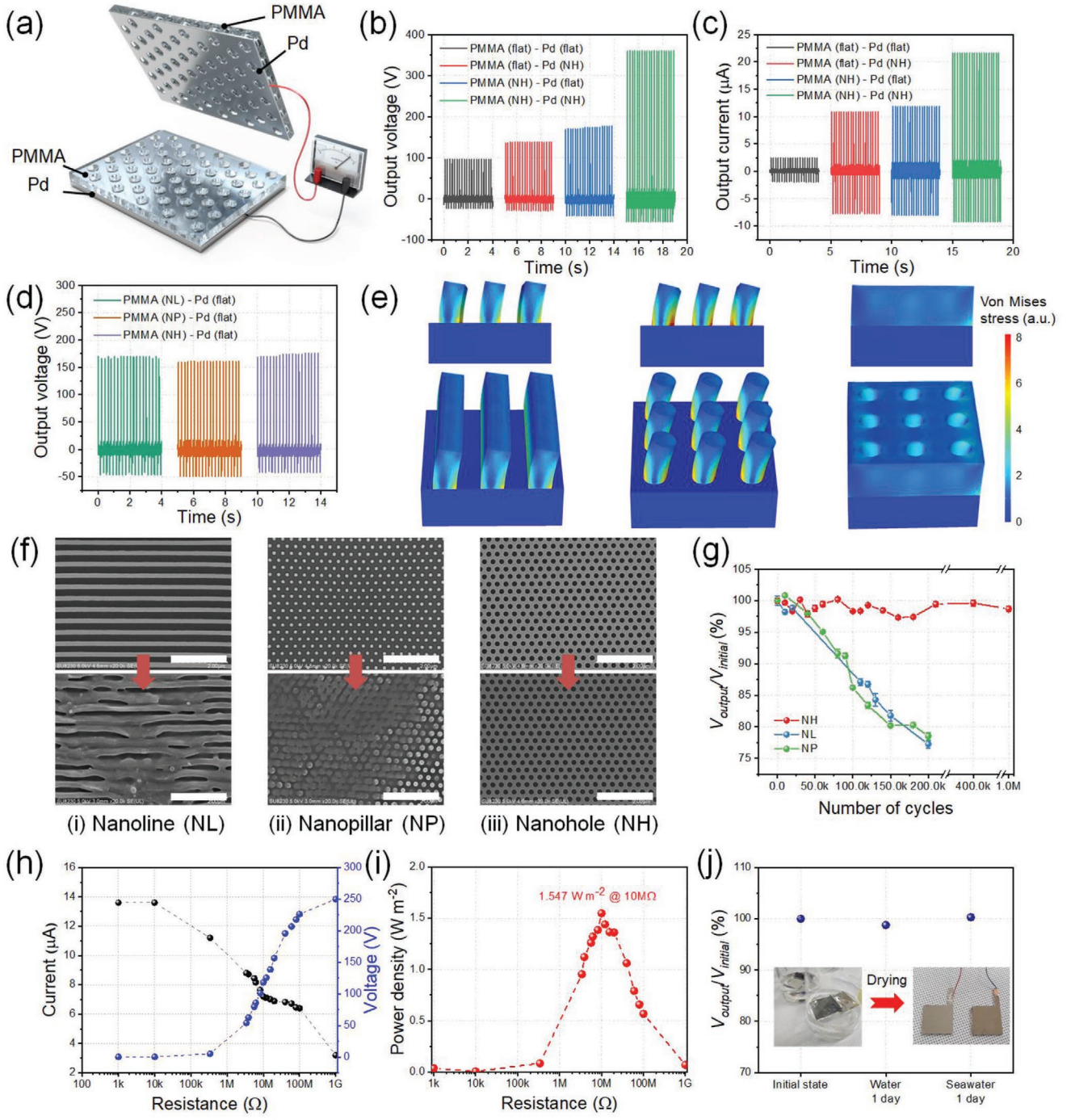

Figure 2. a) Schematic of the developed AR-TENG. b) Output voltage and c) output current obtained for different surface morphologies on each AR-TENG side. d) Output voltages of one-side-nanopatterned AR-TENGs with NL, NP, and NH patterns. e) Results of mechanical stress analysis under uniform shear and normal stress obtained by the numerical simulation for different nanopatterns using the finite element method. Effects of cyclic contacts on f) the top-view SEM images of AR-TENGs with different patterns and g) the output voltage divided by the initial output voltage up to 200 000 cycles (NL and NP) and 1000000 cycles (NH). In the mechanical stability test, AR-TENGs with the nanopatterns on both conductor and dielectric sides were used. h) Voltage and current and i) the corresponding power density of the NH-patterned AR-TENG as functions of applied external resistance. j) Effects of immersion into deionized water and seawater for 1 d on the output voltage of the NH-patterned AR-TENG. The size of scale bars in (f) is 2 μm.

performance and mechanical stability. Figure 2d presents the performances of AR-TENGs with nanoline (NL), nanopillar (NP), and NH patterns, which reveals that these patterns had similar positive effects. Figure S6a,b (Supporting Information) shows the charge density comparison results to investigate the effects of the nanopattern and nanopattern shape. Figure S7

(Supporting Information) presents the top- and side-view SEM images of the NH, NL, and NP patterns. However, the NH pattern show the highest mechanical stability at a constant applied force per unit area when shear and normal forces are applied to the top surface of each pattern in the numerical simulation (Figure 2e); the detailed simulation parameters are described in Figure S8 (Supporting Information). The NH pattern exhibited the largest moment of inertia for bending and thus allowed the stress to be uniformly distributed, i.e., the amount of deformation (bending) and maximum stress were small under the applied external shear force. Therefore, AR-TENGs with the NL and NP patterns exhibited 20% degradation of output voltage after 200000 cycles as compared to the initial state due to mechanical wear. On the other hand, the NH-patterned AR-TENG has an excellent mechanical stability against the applied shear force, and it could maintain its superior energy harvesting performance after the long-term operation of 1 000 000 cycles with less than 2% of degradation (Figure 2g). The NH-patterned AR-TENG has excellent mechanical stability against the applied shear force, and this can maintain its superior energy harvesting performance after the long-term operation of 1 000 000 cycles. Therefore, further experiments, which include those probing the effects of the applied external resistance on performance, were performed for the NH-patterned AR-TENG. As shown in Figure 2h,i, the peak instantaneous power density reached 1.547 W m^{-2} under an external resistance of 10 MΩ. We evaluated the effects of the contact force and vibration frequency of the shaker (Figure S9, Supporting Information) and tested the chemical stability of the AR-TENG by immersing it into pure water and seawater that has several ions such as chloride (Cl^-), sodium (Na^+), and sulfate ($SO^2{}_4^-$) (Figure 2j). Neither of the two immersions affected the performance of the AR-TENG, which was ascribed to the superior chemical stability of its constituents.

2.3. Recycling of the AR-TENG

Upon damage or expiry, the AR-TENG can be disassembled by simple immersion into acetone. PMMA is dissolved in acetone and reprocessed, while Pd is reused as a thin film form; further details are provided in Figure S10 (Supporting Information). All AR-TENG components, which include the electrodes, can be recycled. **Figure 3** shows the results of the AR-TENG recycling experiments. First, the device is decomposed into raw PMMA and Pd using the process shown in Figure S9 (Supporting Information), and the recycled PMMA and Pd are probed by Fourier-transform infrared (FTIR) spectroscopy and X-ray photoelectron spectroscopy (XPS), respectively. The FTIR spectrum of the recycled PMMA is identical to that of the original PMMA (e.g., 1150 to 1250 cm^{-1} for the C—O—C stretching vibration, 1240 and 752 cm^{-1} for the α-methyl group vibrations, 840 and 981 cm^{-1} for the characteristic absorption vibration of PMMA, 1732 cm^{-1} for the acrylate carboxyl group, 1444 cm^{-1} for the bending vibration of the C—H bonds of the $-CH_3$ group, and 2952 and 2997 cm^{-1} for the C—H bond stretching vibrations of the $-CH_3$ and $-CH_2-$ groups, respectively), as shown in Figure 3b. The XPS spectrum of the original Pd 3d is fitted to two pairs of asymmetric peaks as shown in Figure 3c. The intense doublet peaks (i.e., Pd $3d_{3/2}$ (341.0 eV) and Pd $3d_{5/2}$ (335.8 eV)) belong to Pd^0, and the weak peaks (i.e., Pd $3d_{3/2}$ (342.5 eV) and Pd $3d_{5/2}$ (337.3 eV)) are attributed to Pd^{2+} species such as PdO and $Pd(OH)_2$. The tendency of the XPS spectrum of recycled Pd 3d is identical to those of the original Pd metal and there are no additional peaks due to chemical damages or oxidation, which means Pd does not generate any chemical reaction during recycling. In addition, the results of XRD analysis confirm that the recycled Pd has identical crystalline structures with the as-deposited Pd on nanopatterned PMMA substrate before the recycling process (Figure S11, Supporting Information), which are attributed to the high chemical stability of Pd. The recycled materials are used to construct AR-TENGs using the original fabrication process. Figure 3d shows the performance of the re-fabricated AR-TENG was almost the same as that of the original device, with the related differences in the peak output voltage and current equaling 1–3%. Therefore, we concluded that upon damage or expiry, the AR-TENG can be re-fabricated without the need for additional materials or the generation of waste.

Then, we recycled it into a PCF to demonstrate the recyclability and broad applicability of our AR-TENG. We fabricated a metallic PCF with NH arrays as the developed method can be applied to fabricate devices with various combinations of nanopatterned PMMA and different noble metals. The working principle of the PCF is based on the extraordinary optical transmission phenomenon,[36] and the color depends on the hole size and pitch of the pattern. Therefore, a Si master mold with four different NH patterns was designed and fabricated to realize the three primary colors of light (i.e., red, green, and blue) and purple, which is a combination of the three primary colors (Figure S12, Supporting Information). In this design, Ag was used instead of recycled Pd for the PCF because of the excellent plasmonic characteristics of the former metal, which is more conductive than Au and more resistant to oxidation by ambient air than Al.[36] Figure S13a (Supporting Information) illustrates the recycling of the AR-TENG, which shows that it was immersed into acetone, the PMMA film was re-fabricated, and a thin Ag film was deposited by e-beam evaporation on the PUA mold. Nanotransfer printing (nTP) was applied instead of NIL. The previously developed nTP method was used to transfer the Ag thin film from the PUA mold to the PMMA mold at temperatures above the T_g of the latter.[33] Under these conditions, PMMA is deformed by the external pressure and mechanically interlocked with the Ag film (Figure S13a, Supporting Information), with further details provided in our previous paper.[33] Although NIL is suitable for PCF fabrication, it decreases the transmittance of incident light because of the inevitable formation of a metal film on both the top surface of the trench and pillar of the nanopattern. As nTP was used herein, the Ag on the PUA pillar was transferred to the PMMA film, whereas the Ag on the PUA trench was not (Figure S13b, Supporting Information). Figure S14 (Supporting Information) presents the SEM images that correspond to each processing step and pattern. Figure 3e shows the fabricated four-color PCF, which reveals sharp optical transmittance peaks (corresponding to red, green, blue, and purple) at the corresponding wavelengths (Figure 3f). SEM images of the four different NH patterns are presented in Figure 3g. Thus, we concluded that

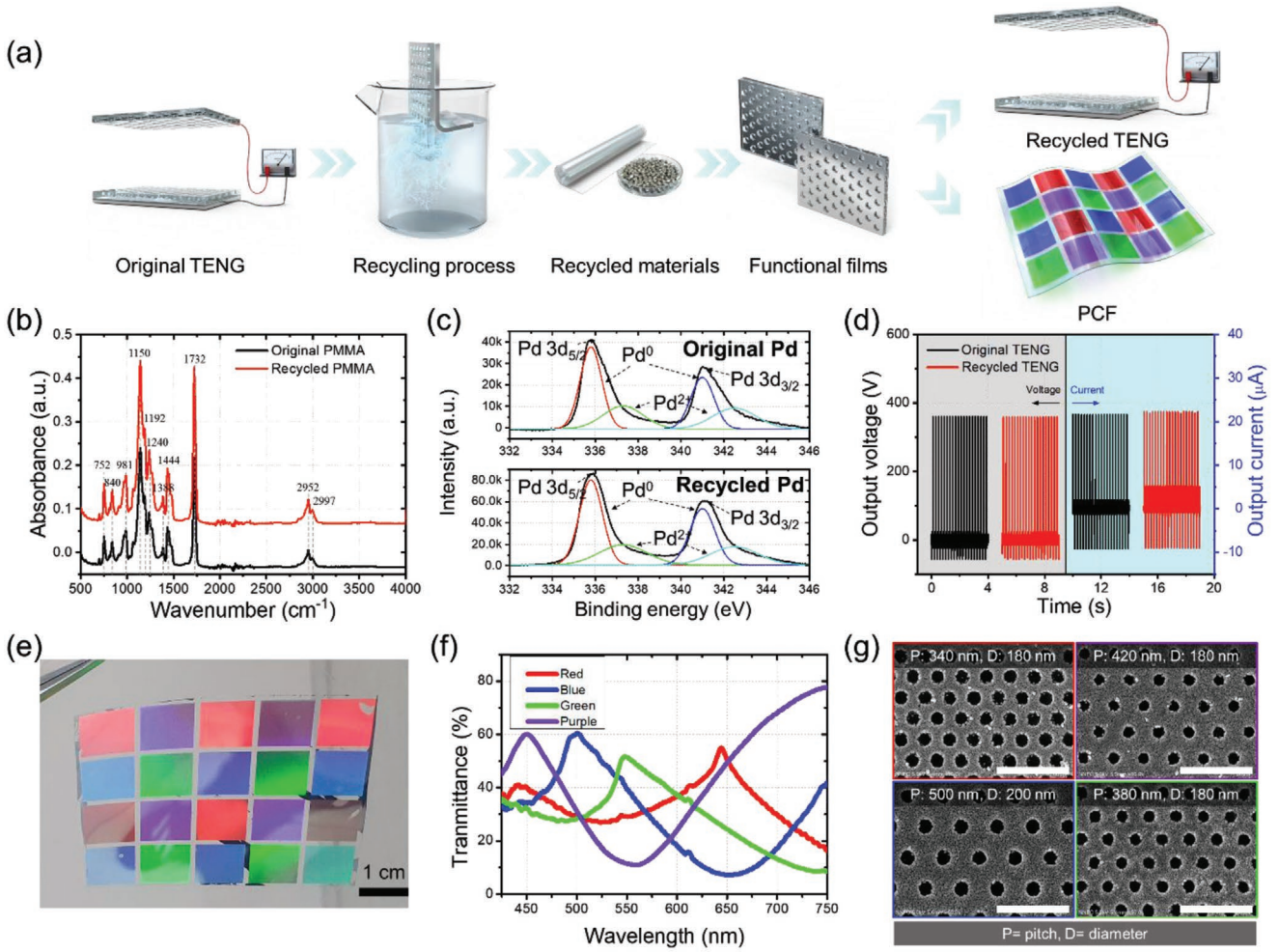

Figure 3. a) Schematic of the AR-TENG recycling process involving disassembly and re-assembly for the re-fabrication of the AR-TENG and PCF. b) FTIR spectra of the PMMA film recorded before and after recycling. c) XPS spectra of Pd recorded before and after recycling. d) Effects of recycling on the output voltage and current of the AR-TENG. e) Photographic image and f) transmittance spectra of the fabricated four-color PCF. g) Top-view SEM images of the four different PCF regions representing different colors. The size of scale bars in (g) is 1 μm.

the AR-TENG could not only be re-fabricated but also the other optical or electrical devices such as the PCF could be fabricated using the spent AR-TENG without the need for additional materials or the generation of waste. The AR-TENG developed in this study has a great advantage because not only can it harvest renewable ocean energy but the device itself can be recycled without any generation of e-waste.

2.4. Characterization of Energy Harvesting System Based on the AR-TENG

Figure 4a,b shows a schematic and photographic images of the energy harvesting system that comprises the large-area AR-TENG (8 cm × 8 cm), an elastomer pad, and an additional weight. The elastomer pad was used to ensure the conformal contact of each side of the large-area AR-TENG, which increases the effective contact area and improves the output power of the energy harvesting system because rigid-to-rigid surface contact dramatically reduces the actual contact area,[37] whereas the additional weight is used to regulate the contact condition depending on the wave amplitude, as discussed below. The energy harvesting system was integrated into a floatable box that imitated a buoy in the ocean and floated in a wave pool (Figure 4c and Figure S15a, Supporting Information). In the floatable box, the AR-TENG can generate the renewable electricity utilizing the periodic contact and separation motion between two triboelectric materials with a one-dimensional spring-mass system under the input motion of ocean waves (Videos S1 and S2, Supporting Information). We conducted experiments with additional weights at different frequencies and amplitudes to determine the optimal conditions of the additional weights for improving the energy harvesting performance of the integrated buoy system. The peak output voltage at all the different amplitude and frequency cases increased until a certain point and then decreased as the mass of the extra weight increased (Figure 4d). This behavior was explained by the fact that the additional weight determines the initial (neutral) distance between each side of the AR-TENG because of the deformation of the spring. A proper

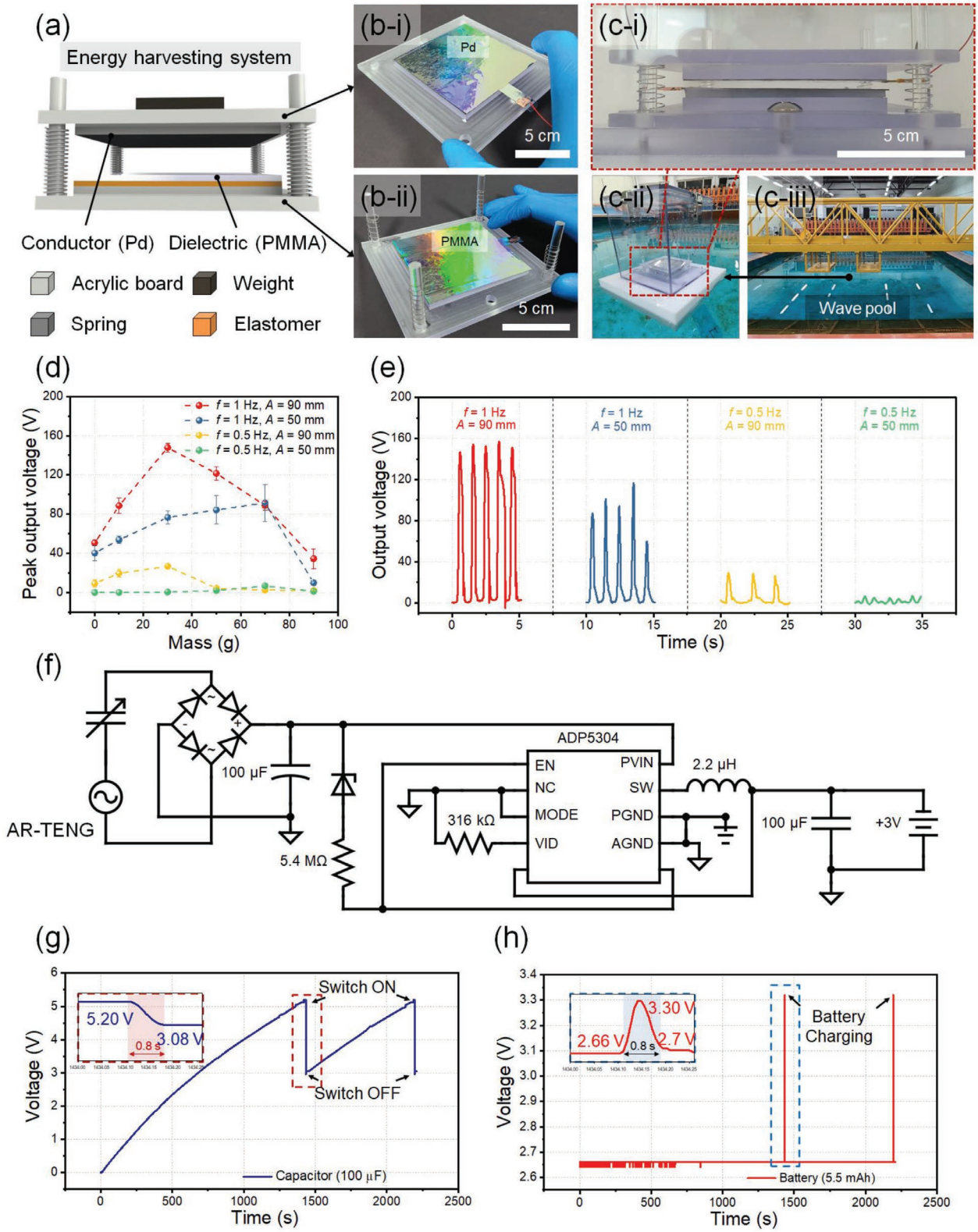

Figure 4. a) Schematic and b) photographic images of the developed ocean energy harvesting system. c) Photographic images of the developed system in a wave pool that can generate water waves to mimic ocean environments. d) Peak output voltages of energy harvesting system obtained for various weights under diverse wave conditions generated at different actuator frequencies (*f*) and amplitudes (*A*). e) Output voltages using optimal weights in various wave conditions. f) Electrical circuit used to charge a commercial Li-ion battery or drive a commercial Arduino board at a constant voltage. The voltage profiles of g) the capacitor and h) battery upon constant charging by the AR-TENG.

weight increases the output voltage by facilitating contact with the TENG even for a small mechanical input, whereas an overly heavy weight decreases the output voltage by reducing the separation distance. Therefore, one should consider the strong dependence of the optimized mass on the state of the wave and evaluate the effects of actuator input frequency and amplitude to optimize the energy harvesting system. A detailed discussion of the weight effect on the output voltage is provided in Supporting Information. Figure 4e shows the output voltages of the developed energy harvesting system when optimal additional weight is used in various wave conditions of the wave pool. The output voltage is 155 and 87 V, respectively, when the applied frequency is 1 Hz with the applied amplitude of 90 mm and 50 mm; the output voltage was 28 and 6.6 V when the applied frequency of 0.5 Hz with the applied amplitude of 90 mm and 50 mm, respectively.

An electrical circuit for charging a commercial Li-ion battery was developed (Figure 4f and Figure S15b, Supporting Information) and used to characterize the charging capacity of the energy harvesting system because the capacitor used for demonstrating TENGs has a limitation of a fast discharge rate, which limits the use for the sustainable ocean monitoring system. For battery charging, the AC electrical output harvested by the AR-TENG was first converted into a DC signal by a rectifier and then used to charge a 100 μF capacitor. The electrons automatically passed through the Zener diode when the voltage of the capacitor reached 5.2 V; the switch connected to the regulator adopted the "on" state (Figure 4g). The regulator decreased the voltage to 3.3 V for the constant-voltage charging of the battery using the harvested electrical energy. As shown in Figure 4h, the voltage of the battery in the initial state equaled 2.66 V, and it instantaneously increased to 3.3 V after connection to the regulator; then, it reached 2.7 V after charging was complete. The battery voltage increase of 0.04 V upon charging indicates that the battery was successfully charged by electrical energy harvested by the AR-TENG, with the amount of charged energy determined as 814.04 μW s. The regulator was powered by the harvested energy (7.9% of the transmitted energy was consumed by the voltage drop in the regulator), i.e., the overall electrical circuit system was exclusively powered by renewable energy. The total amount of charged energy in the battery was determined from the voltage profiles of the capacitor and the battery and from the current profile of the regulator (Figure S16, Supporting Information). A detailed discussion of battery charging capacity is provided in the Supporting Information. Further, the developed electrical circuit could not only charge the battery, but also temporarily operate a commercial Arduino board (Figure S15b, Supporting Information); therefore, it was deemed to be a suitable self-powered microcontroller system that could operate wireless sensors and periodically transmit signals for a sustainable ocean monitoring system.

The battery charging demonstration of the proposed energy harvesting system based on the AR-TENG could pave the way for the sustainable operation of renewable energy. Further, the output power can be improved by arranging multiple AR-TENGs with mechanically robust and high-performance properties in the ocean for the sensor networks of the ocean monitoring system.

2.5. Applications of the AR-TENG to the Ocean Monitoring Systems

We integrated it into a buoy-type ocean monitoring system and a life jacket to demonstrate the practical applicability of the developed energy harvesting system. The intelligent buoy was designed to monitor the condition of seawater and regularly transmit it to land through wireless communication, which comprises the AR-TENG with a battery charging module, a wireless communication module, and four (pH, salinity, temperature, and oil leakage) sensors (**Figure 5**a,b and Figure S17, Supporting Information). Among these four sensors, three of them (pH-, salinity-, and temperature sensors) measure the representative monitoring parameters of seawater, and the other (oil leak sensors) detects the oil leakage from vessels on the sea. As indicated in Figure 5c and Video S3 (Supporting Information), each parameter is successfully measured by the sensors when brine, acidic buffer solution, hot water, and oil are successively added to the seawater; the calculated power consumption of each component is described in Table S1 (Supporting Information). The intelligent life jacket can automatically or manually transmit an emergency signal (Figure 5d) comprising the AR-TENG, a battery-charging module, a wireless communication module, and an integrated GPS sensor (Figure 5e). In this case, the AR-TENG can be operated not only by ocean wave energy, but also by human motion (Figure 5f). The GPS sensor transmitted an emergency signal including location details when the Zener diode switch was turned on, i.e., when the life jacket floated on seawater or was activated manually (Figure 5g and Video S4, Supporting Information). Thus, the developed energy harvesting system was found to hold great promise for ocean monitoring systems (e.g., intelligent buoys and life jackets).

3. Conclusions

In this study, a high-performance and mechanochemically stable AR-TENG was developed and used to fabricate a sustainable ocean energy harvesting system. The AR-TENG successfully secured excellent mechanical and chemical durability by designing the NH structure with a large moment of inertia against bending and applying chemically stable materials, respectively. To the best of our knowledge, the AR-TENG is the first to be ever reported, and it exhibits the highest performance and durability among the known recyclable or disposable TENGs (Table S2, Supporting Information). In addition, the entire device, including electrodes, could be easily disassembled in acetone and recycled to reduce the generation of e-waste as the AR-TENG contained only a thermoplastic polymer (PMMA) and a noble metal (Pd). Moreover, the AR-TENG could be recycled as a PCF using the nTP method; the obtained PCF demonstrated four clear colors (red, green, blue, and purple). Then, the AR-TENG was subsequently integrated into a buoy-type ocean monitoring system and an intelligent life jacket. The intelligent buoy included four different sensors and could monitor oil leakage and the pH, salinity, and temperature of seawater, whereas the intelligent life jacket contained a GPS sensor and could notify an emergency of the wearer to land. In both cases, the battery was continuously charged by the energy

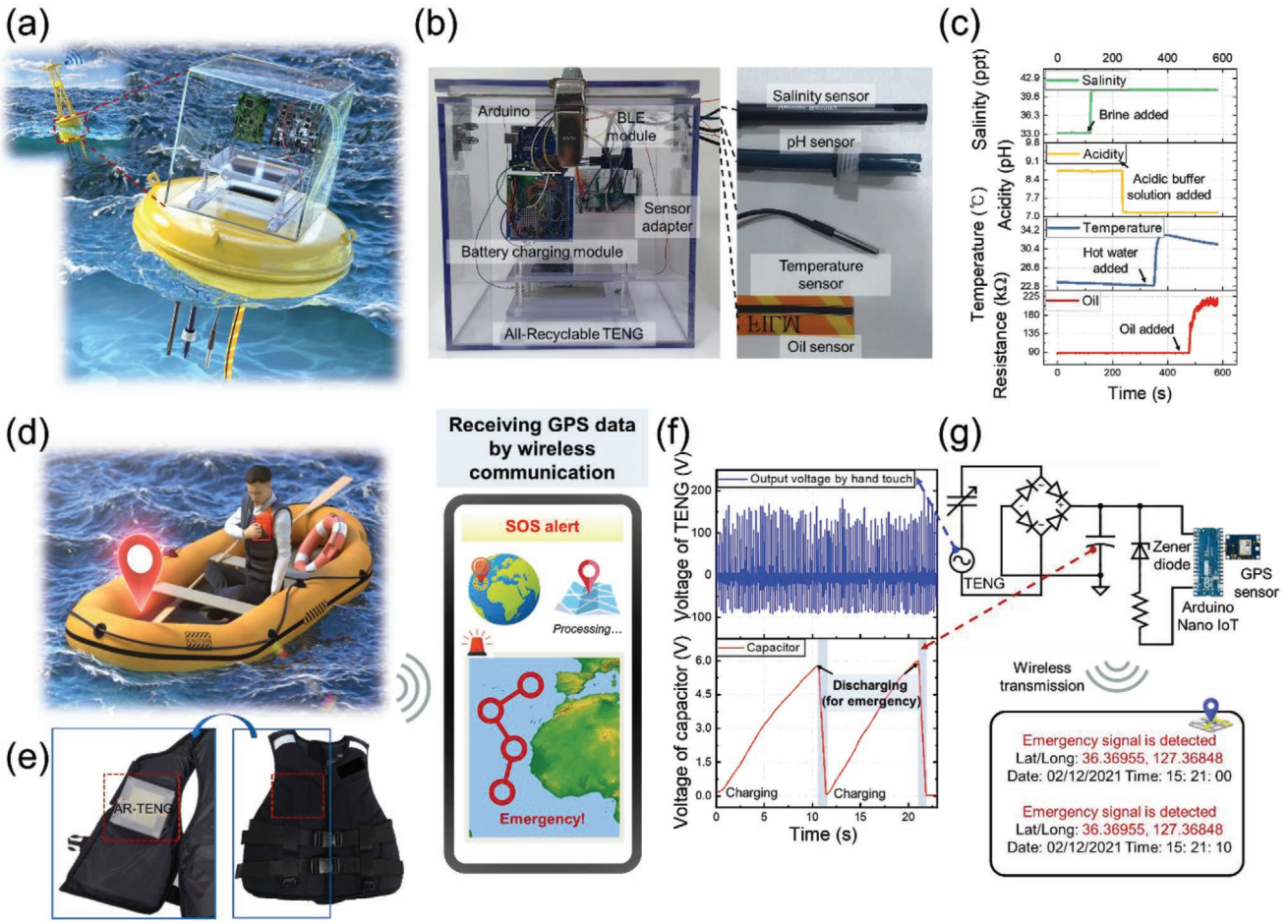

Figure 5. a) Schematic and b) photographic images of the intelligent buoy including a battery charging module, a wireless communication module, and four (pH, salinity, temperature, and oil leakage) sensors. c) Results of the intelligent buoy evaluation under different ocean conditions. In this experiment, brine, acidic buffer solution, hot water, and oil were added to the seawater successively. d) Schematic and e) photographic images of the intelligent life jacket which includes the AR-TENG, a battery-charging module, wireless communication module, and GPS sensor. f) The voltage of the AR-TENG by hand touch and capacitor integrated into the intelligent life jacket. g) Schematic of the electrical circuit for triggering the GPS sensor using the harvested energy by the AR-TENG and the screen of a mobile device that can receive GPS data from the intelligent life jacket by wireless communication.

supplied from the AR-TENG for the sustainable operation of the ocean monitoring system. To the best of our knowledge, this study provides for the first time a fully integrated and practical ocean monitoring system including a TENG, capacitor charging circuit, battery charging circuit, sensors, and wireless communication system (Table S3, Supporting Information).

Despite the above success, there remain challenges to be addressed. First, a more environmentally friendly combination of polymers and solutions needs to be developed without degrading the performance. Although acetone is a preferred green solvent[38] even in the pharmaceutical industry, it is somewhat toxic.[39] Therefore, the development of AR-TENGs that can be recycled in a more environmentally friendly manner will help reduce the generation of chemical waste. Second, the realization of a perfect AR-TENG requires the availability of recyclable electric wires and packing materials. Herein, recycling was limited to polymers and electrodes on the TENG structure, and it was not applied to the electric wires and packaging materials.

However, we believe that results presented herein will help resolve global environmental problems such as climate change[40,41] and ozone depletion through the efficient and green harvesting of wasted mechanical energy; we expect them to pave the way to harvest renewable energy beyond that of oceans, e.g., wind and rain energy.

4. Experimental Section

AR-TENG Fabrication and Recycling: A Si master was prepared by krypton fluoride (KrF) lithography to fabricate functional films comprising nanopatterned PMMA and Pd thin films. For polymer mold replication, RM-311 resin (polyurethane, Minuta Technology Co., Ltd., Korea) was poured onto the prepared Si master and covered by a UV-transparent polyethylene terephthalate film. Pressure was applied to the resin using a hand roller to facilitate the complete penetration of this resin into the nanopatterns of the Si master. Then, the resin was cured under illumination with UV light and separated from the Si master to afford a polymer mold. This process can be conducted repeatedly, and various nanopatterns can be fabricated using various Si masters. The detailed

fabrication of the polymer mold from the Si master was described in a previous work.[42,43] The surface of the Si master had to be treated with trichloro(1H,1H,2H,2H-perfluorooctyl)silane to facilitate polymer mold detachment. Then, the nanopatterned PUA mold was used to pattern the PMMA film at 110 °C (i.e., at a temperature above the T_g of PMMA) and 5 bar for 10 min. Two nanopatterned PMMA films were fabricated using repeated NIL. Next, a 50 nm thick Pd layer was deposited using an e-beam evaporator (Daeki Hi-Tech Co., Ltd., Korea) on one side of both films: One layer was deposited on the back of the PMMA film (flat part), and the other was deposited on the front of the other PMMA film (patterned part) to afford the electrodes of the dielectric and conductor parts of the AR-TENG, respectively. The two functional films were used on each side of the AR-TENG; both films comprising PMMA and Pd (total thickness = 30 µm) were attached to a thick PMMA substrate (thickness = 1 mm) and electric wires were connected using Ag paste. Fabricated samples were evaluated by field-emission scanning electron microscopy (FE-SEM; Sirion, FEI, the Netherlands) and focused ion-beam scanning electron microscopy (FIB-SEM; Helios Nanolab, FEI, the Netherlands). For recycling, the AR-TENG was detached from the thick PMMA substrate, and the two functional films were immersed into acetone for 20 min. The floated Pd film was removed using a tweezer and reused as a source for the e-beam evaporation. The remaining acetone solution of PMMA was placed in a vacuum oven and heated for 5 h at 50 °C to evaporate acetone. The remaining PMMA was reformed as a thin film by repeated hot pressing at 140–200 °C and 3–5 bar for a new thermal NIL process.

AR-TENG Characterization: Characterization was performed for a device with the dimensions of 3 cm × 3 cm. A digital phosphor oscilloscope (DPO2002B, Tektronix, USA), a high-voltage probe with an input impedance of 40 MΩ (P5100A, Tektronix, USA), and a pre-current amplifier (SR570, Stanford Research Systems, USA) were used to measure the output voltage and current. A system electrometer (Model 6514, Keithley Instrument, USA) was used to measure the output voltage, current, and transferred charge. A dual-channel arbitrary function generator (AFG3022, Tektronix, USA) was used to generate a sinusoidal function for the shaker excitation. A power amplifier (Type BAA 120, TIRA, Germany) was used because a high voltage and current were required to drive the shaker. A vibration test system (TV 51075, TIRA, Germany) was used as a shaker to demonstrate the contact-separation mode of the AR-TENG. Contact force measurements were performed using a force sensor (1051V2, Dytran Instruments, USA) powered by a sensor signal conditioner (Model 480E09, PCB Piezotronics, USA). The output triboelectric performance of the AR-TENG was investigated at different forces (1, 2, 4, 6, and 8 N) and frequencies (1–7 Hz), as shown in Figure S9 (Supporting Information). Thereafter, the triboelectric performance was characterized at an operating force of 8 N and a frequency of 5 Hz. The long-term stability test was conducted at an operating force of 8 N and a frequency of 10 Hz. Electrostatic simulation was conducted to demonstrate the operating principle of the AR-TENG in the open circuit condition using COMSOL Multiphysics. The finite element method was used in conjunction with COMSOL Multiphysics software to compare the mechanical stabilities of PMMA films with different surface morphologies (NL, NP, and NH patterns). For comparison, the unit cell size was set to 0.9 µm × 0.9 µm, and the same normal and shear force per unit areas were set to be exerted on the surface; the von Mises stresses were compared.

Recycling and PCF Fabrication: The PCF was fabricated using previously developed NIL and nTP processes, with the AR-TENG recycling performed as described above. The nTP process was conducted using the recycled PMMA film and Ag pellets. A Si master mold with four different NH pattern types was designed and fabricated by KrF lithography, and a nanopatterned PUA replica was prepared by the abovementioned process for the PUA mold fabrication. A 40 nm thick layer of Ag was deposited on the PUA mold using an e-beam evaporator. The nanopatterned PUA mold with Ag was transferred onto the PMMA film using a previously developed nTP technique, namely heating above the T_g of PMMA (110 °C) at 6 bar for 5 min. After 5 min cooling, the PUA mold was separated from the PMMA film to obtain an Ag nanopattern on the PMMA film (i.e., the PCF). The optical transmittance of the resulting PCF was characterized using a spectrometer (QE Pro 6000, Ocean Optics, USA).

Fabrication and Characterization of the Ocean Energy Harvesting System with a Battery Charging Circuit: Each NH-patterned thin film comprising PMMA and Pd (total thickness = 30 µm) was attached to the thick PMMA substrate for proper rigidity. A simple mechanical spring system utilizing an AR-TENG with a size of 8 cm × 8 cm was designed to harvest ocean wave energy. A soft elastomer pad fabricated using Ecoflex (Ecoflex 0030, Smooth-On, USA) was placed on one side of the AR-TENG for conformal contact. A mechanical spring and additional weight were systematically used throughout the experiments. The output voltages of the ocean energy harvesting system with a battery charging circuit were examined in the wave pool with the size of 11 × 10 m. In this experiment, the performance of the developed harvesting system was evaluated as functions of the amplitude (50 and 90 mm) and frequency (0.5 and 1 Hz) of the actuator that generates the water wave (Figure S12a, Supporting Information).

An ultralow-power step-down regulator with input voltage monitoring and regulation functions (ADP5304, Analog Devices, USA) was used to charge a commercial Li-ion battery (MS621FE, Seiko Instruments Micro Energy, Japan) with a nominal capacity of 5.5 mAh using a constant-voltage charging method. The regulator converted the irregular output voltage of the capacitor into a constant voltage. In addition, a Zener diode (TZX3V0B-TR, Vishay Semiconductors, USA) was used to adjust the threshold voltage of a switch connected to the regulator to 5.2 V.

Construction of the Ocean Monitoring System: The ocean monitoring system was constructed using an Arduino Uno board, a Bluetooth module (HC-05), the customized battery charging circuit, the AR-TENG, and additional sensors. For the intelligent buoy, a salinity sensor (Vernier, USA), a pH sensor (Vernier, USA), a temperature sensor (DS18B20), and an oil leakage sensor (LK16-T2-2000HD, YUMINST, Korea) were used, while a GPS sensor (GY-NEO6MV2) was used for the intelligent life jacket. During the demonstration of real-time monitoring systems, the overall systems were powered by the previously charged battery for demonstrating the feasibility of ocean monitoring based on the proposed sensors and wireless data communication while the battery was continuously charged by the AR-TENG.

Supporting Information

Supporting Information is available from the Wiley Online Library or from the author.

Acknowledgements

J.A. and J.-S.K. contributed equally to this work. This work was supported by Creative Research Initiative Program (2015R1A3A2028975) and funded by the National Research Foundation of Korea (NRF), the Defense Acquisition Program Administration and the Agency for Defense Development (ADD) in Korea under the contract UD200011DD, by the Center for Advanced Meta-Materials (CAMM) funded by the Ministry of Science, ICT, and Future Planning as Global Frontier Project (CAMM No. 2014M3A6B3063707), Institute of Information & Communications Technology Planning & Evaluation (IITP) grant funded by the Korea government (MSIT) (No. 2020-0-00914, Development of hologram printing downsizing technology based on holographic optical element(HOE)), and by a National Research Foundation of Korea (NRF) grant funded by the Korea government (MSIT) [No. 2021R1A2C3008742]. This research was a part of the project titled "Development of Management Technology for HNS Accident" (No. D11502815H480000140 2015034016), funded by the Ministry of Oceans and Fisheries, Korea.

Conflict of Interest

The authors declare no conflict of interest.

Data Availability Statement

Research data are not shared.

Keywords

intelligent buoys, life jackets, ocean energy harvesting, ocean monitoring systems, recyclable triboelectric nanogenerators, renewable energy

Received: April 20, 2022
Published online: June 9, 2022

[1] J. Yu, X. Wang, M. Zhou, Q. Wang, *Energy Environ. Sci.* **2019**, *12*, 2672.
[2] M. Amer, E. Z. Wojcik, C. Sun, R. Hoeven, R. Hoeven, J. M. X. Hughes, M. Faulkner, I. S. Yunus, S. Tait, L. O. Johannissen, S. J. O. Hardman, D. J. Heyes, G. Q. Chen, G. Q. Chen, M. H. Smith, P. R. Jones, H. S. Toogood, N. S. Scrutton, N. S. Scrutton, N. S. Scrutton, *Energy Environ. Sci.* **2020**, *13*, 1818.
[3] N. A. Shepelin, P. C. Sherrell, E. Goudeli, E. N. Skountzos, V. C. Lussini, G. W. Dicinoski, J. G. Shapter, A. V. Ellis, *Energy Environ. Sci.* **2020**, *13*, 868.
[4] O. J. Guerra, J. Eichman, P. Denholm, *Energy Environ. Sci.* **2021**, *14*, 5132.
[5] J. S. Kim, J. Kim, J. N. Kim, J. Ahn, J. H. Jeong, I. Park, D. Kim, I. K. Oh, *Adv. Energy Mater.* **2022**, *12*, 2103076.
[6] C. Rodrigues, D. Nunes, D. Clemente, N. Mathias, J. M. Correia, P. Rosa-Santos, F. Taveira-Pinto, T. Morais, A. Pereira, J. Ventura, *Energy Environ. Sci.* **2020**, *13*, 2657.
[7] M. Heacock, C. B. Kelly, K. A. Asante, L. S. Birnbaum, Å. L. Bergman, M. N. Bruné, I. Buka, D. O. Carpenter, A. Chen, X. Huo, M. Kamel, P. J. Landrigan, F. Magalini, F. Diaz-Barriga, M. Neira, M. Omar, A. Pascale, M. Ruchirawat, L. Sly, P. D. Sly, M. van den Berg, W. A. Suk, *Environ. Health Perspect.* **2016**, *124*, 550.
[8] Z. Bai, Y. Xu, J. Li, J. Zhu, C. Gao, Y. Zhang, J. Wang, J. Guo, *ACS Appl. Mater. Interfaces* **2020**, *12*, 42880.
[9] S. Parandeh, M. Kharaziha, F. Karimzadeh, *Nano Energy* **2019**, *59*, 412.
[10] L. Zhang, Y. Liao, Y. C. Wang, S. Zhang, W. Yang, X. Pan, Z. L. Wang, *Adv. Funct. Mater.* **2020**, *30*, 2001763.
[11] L. Chen, C. Yu, C. Shen, C. Zhang, L. Liu, K. Shen, X. Tang, Y. Chen, *J. Soils Sediments* **2010**, *10*, 359.
[12] Y. Lu, X. Li, J. Ping, J. song He, J. Wu, *Adv. Mater. Technol.* **2020**, *5*, 1900905.
[13] Q. Liang, Q. Zhang, X. Yan, X. Liao, L. Han, F. Yi, M. Ma, Y. Zhang, *Adv. Mater.* **2017**, *29*, 1604961.
[14] W. Xu, H. Zheng, Y. Liu, X. Zhou, C. Zhang, Y. Song, X. Deng, M. Leung, Z. Yang, R. X. Xu, Z. L. Wang, X. C. Zeng, Z. Wang, *Nature* **2020**, *578*, 392.
[15] X. Liang, T. Jiang, G. Liu, Y. Feng, C. Zhang, Z. L. Wang, *Energy Environ. Sci.* **2020**, *13*, 277.
[16] L. Xu, L. Xu, J. Luo, Y. Yan, B. E. Jia, X. Yang, Y. Gao, Z. L. Wang, *Adv. Energy Mater.* **2020**, *10*, 2001669.
[17] S. Nie, H. Guo, Y. Lu, J. Zhuo, J. Mo, Z. L. Wang, *Adv. Mater. Technol.* **2020**, *5*, 2000454.
[18] Q. Zheng, Y. Zou, Y. Zhang, Z. Liu, B. Shi, X. Wang, Y. Jin, H. Ouyang, Z. Li, Z. L. Wang, *Sci. Adv.* **2016**, *2*, e1501478.
[19] J. Zhang, S. Hu, Z. Shi, Y. Wang, Y. Lei, J. Han, Y. Xiong, J. Sun, L. Zheng, Q. Sun, G. Yang, Z. L. Wang, *Nano Energy* **2021**, *89*, 106354.
[20] Q. Zhou, K. Lee, K. N. Kim, J. G. Park, J. Pan, J. Bae, J. M. Baik, T. Kim, *Nano Energy* **2019**, *57*, 903.
[21] G. Knutsen, *Mar. Pollut. Bull.* **1983**, *14*, 112.
[22] K. Xia, J. Fu, Z. Xu, *Adv. Energy Mater.* **2020**, *10*, 2000426.
[23] H. Wang, Z. Fan, T. Zhao, J. Dong, S. Wang, Y. Wang, X. Xiao, C. Liu, X. Pan, Y. Zhao, M. Xu, *Nano Energy* **2021**, *84*, 105920.
[24] L. Liu, X. Yang, L. Zhao, H. Hong, H. Cui, J. Duan, Q. Yang, Q. Tang, *ACS Nano* **2021**, *15*, 9412.
[25] G. Liu, H. Guo, S. Xu, C. Hu, Z. L. Wang, *Adv. Energy Mater.* **2019**, *9*, 1900801.
[26] M. Xu, T. Zhao, C. Wang, S. L. Zhang, Z. Li, X. Pan, Z. L. Wang, *ACS Nano* **2019**, *13*, 1932.
[27] Z. L. Wang, T. Jiang, L. Xu, *Nano Energy* **2017**, *39*, 9.
[28] P. Chen, J. An, S. Shu, R. Cheng, J. Nie, T. Jiang, Z. L. Wang, *Adv. Energy Mater.* **2021**, *11*, 2003066.
[29] X. Wei, Z. Zhao, C. Zhang, W. Yuan, Z. Wu, J. Wang, Z. L. Wang, *ACS Nano* **2021**, *15*, 13200.
[30] D. Y. Kim, H. S. Kim, D. S. Kong, M. Choi, H. B. Kim, J. H. Lee, G. Murillo, M. Lee, S. S. Kim, J. H. Jung, *Nano Energy* **2018**, *45*, 247.
[31] D. Zhang, J. Shi, Y. Si, T. Li, *Nano Energy* **2019**, *61*, 132.
[32] Z. J. Zhao, J. Ahn, S. H. Hwang, J. Ko, Y. Jeong, M. Bok, H. J. Kang, J. Choi, S. Jeon, I. Park, J. H. Jeong, *ACS Nano* **2021**, *15*, 503.
[33] J. Ahn, Z. J. Zhao, J. Choi, Y. Jeong, S. Hwang, J. Ko, J. Gu, S. Jeon, J. Park, M. Kang, D. V. Del Orbe, I. Cho, H. Kang, M. Bok, J. H. Jeong, I. Park, *Nano Energy* **2021**, *85*, 105978.
[34] A. Šutka, K. Malnieks, L. Lapčinskis, P. Kaufelde, A. Linarts, A. Berziņa, R. Zabels, V. Jurķans, I. Gorņevs, J. Blums, M. Knite, *Energy Environ. Sci.* **2019**, *12*, 2417.
[35] H. S. Wang, C. K. Jeong, M. H. Seo, D. J. Joe, J. H. Han, J. B. Yoon, K. J. Lee, *Nano Energy* **2017**, *35*, 415.
[36] S. H. Hwang, Z. J. Zhao, S. Jeon, H. Kang, J. Ahn, J. H. Jeong, *Nanoscale* **2019**, *11*, 11128.
[37] Y. Chen, X. Pu, M. Liu, S. Kuang, P. Zhang, Q. Hua, Z. Cong, W. Guo, W. Hu, Z. L. Wang, *ACS Nano* **2019**, *13*, 8936.
[38] G. Szekely, M. F. Jimenez-Solomon, P. Marchetti, J. F. Kim, A. G. Livingston, *Green Chem.* **2014**, *16*, 4440.
[39] D. Prat, J. Hayler, A. Wells, *Green Chem.* **2014**, *16*, 4546.
[40] L. Pan, E. M. Powell, K. Latychev, J. X. Mitrovica, J. R. Creveling, N. Gomez, M. J. Hoggard, P. U. Clark, *Sci. Adv.* **2021**, *7*, 27.
[41] R. I. Woolway, E. Jennings, T. Shatwell, M. Golub, D. C. Pierson, S. C. Maberly, *Nature* **2021**, *589*, 402.
[42] Z. J. Zhao, J. Ahn, D. Lee, C. B. Jeong, M. Kang, J. Choi, M. Bok, S. H. Hwang, S. Jeon, S. Park, J. Ko, K. S. Chang, J.-W. Choi, I. Park, J. Jeong, *Nanoscale* **2022**, *14*, 1136.
[43] Z. J. Zhao, J. Ahn, J. Ko, Y. Jeong, M. Bok, S. H. Hwang, H. J. Kang, S. Jeon, J. Choi, I. Park, J. H. Jeong, *ACS Appl. Mater. Interfaces* **2021**, *13*, 3358.